Evaluation of TerraSAR-X Observations for Wetland InSAR Application

Sang-Hoon Hong, *Member, IEEE*, Shimon Wdowinski, and Sang-Wan Kim, *Member, IEEE*

***Abstract*—This paper assesses the potential of using space-borne X-band synthetic aperture radar (SAR) data for monitoring water-level changes over wetlands. Our analysis is based on three sets of TerraSAR-X (TSX) observations acquired over South Florida's Everglades wetlands during an eight-month period in 2008. The first set was acquired in single HH polarization stripmap mode over our northern study area, consisting of managed wetlands and urban environments. The second set was acquired in dual-polarization stripmap mode over the western half of the same area, consisting mostly of managed wetlands. The third set was also acquired with dual-polarization stripmap mode over our southern study area, consisting of natural flow fresh- and salt-water wetlands in the southern Everglades. The first data set was used for a proof-of-concept study to verify that X-band data can generate coherent interferograms in wetland areas. Interferometric processing of this data set shows a high level of coherence (> 0.35) over both wetland and urban regions, maintaining interferometric phase in all three interferograms spanning 11 days. Surprisingly, phase is maintained over some of the wetlands even for interferograms spanning 33 days. The other two data sets were used to evaluate interferometric coherence of all four polarization modes and to determine dominant scattering mechanism in each wetland environment. Our results show high coherence values (> 0.4) in all polarization modes, with highest values in HH, then VV, and lowest in HV or VH. Interferograms calculated from multipolarization data show very similar fringe patterns regardless of the polarization type, suggesting that the phase information in all polarization data reflects water-level changes in wetlands and that volume scattering may be less important than commonly believed. We also used the two multipolarization data sets to conduct the Pauli decomposition, finding a strong dependence of scattering mechanism on vegetation type. The high interferometric coherence level of all polarization data suggests that a significant part of the X-band scattered signal interacts with lower sections of the vegetation (trunks and branches), because scattering from wind-affected canopies cannot support such a high coherence level. The high spatial resolution of TSX, combined with its 11-day repeat orbit, makes this X-band sensor surprisingly suitable for wetland interferometric SAR applications.**

Manuscript received February 20, 2009; revised June 1, 2009. First published August 28, 2009; current version published January 20, 2010. This work was supported by the NASA Cooperative Agreement NNX08BA43A (WaterSCAPES: Science of Coupled Aquatic Processes in Ecosystems from Space) Grants.

S.-H. Hong is with the Division of Marine Geology and Geophysics, Rosenstiel School of Marine and Atmospheric Science, University of Miami, Miami, FL 33149-1098 USA, and also with the College of Engineering and Computing, Florida International University, Miami, FL 33174 USA (e-mail: shong@rsmas.miami.edu).

S. Wdowinski is with the Division of Marine Geology and Geophysics, Rosenstiel School of Marine and Atmospheric Science, University of Miami, Miami, FL 33149-1098 USA.

S.-W. Kim is with the Department of Geoinformation Engineering, Sejong University, Seoul 143-747, Korea (e-mail: swkim@sejong.ac.kr).

Color versions of one or more of the figures in this paper are available online at http://ieeexplore.ieee.org.

Digital Object Identifier 10.1109/TGRS.2009.2026895

***Index Terms*—Coherence, interferometric SAR, TerraSAR-X, the Evergaldes, wetlands, X-band.**

I. Introduction

WETLAND interferometric synthetic aperture radar (SAR) (InSAR) is a relatively new application of the InSAR technique, detecting water-level changes in aquatic environments with emergent vegetation [1]–[3]. It provides high-spatial-resolution hydrological observations of wetland and floodplains that cannot be obtained by any terrestrial-based method [1], [4], [5]. Wetland InSAR observations provide high-spatial-resolution monitoring of surface water level and detection of flow patterns and flow discontinuities. These observations can be very useful constraints to high-resolution hydrologic-flow models [4], [5].

In our previous studies, we evaluated the suitability of various data types and acquisition parameters for InSAR wetland application. We have tested a variety of C- and L-band data collected by the ERS-1/2, JERS-1, RADARSAT-1, ENVISAT and ALOS satellites [4]–[7]. Using interferometric coherence, we evaluated the quality of the various InSAR observations obtained over wetlands with various acquisition parameters. A similar study by Lu and Kwoun [8] also used C-band observations acquired over the Louisiana wetlands. They showed that interferometric pair with time interval over several years could be useful for wetland monitoring when the SAR data were acquired at leaf-off season in forest swamp [8]. Other related studies are concerned with the usage of L-band InSAR measurement to detect tide-induced sea-level changes along oyster farms offshore of the Korean coast [9], [10].

Our coherence analyses indicate, in terms of satellite-system parameters, that longer wavelength SAR systems (L-band), horizontal (HH) polarization of the radar pulse, and short repeat orbits provide the best results. Although the results of our analysis favor longer wavelength L-band data, we found that the C-band RADARSAT-1 data with a 24-day repeat cycle and HH polarization is also very useful for the wetland InSAR applications [5]. Nevertheless, previous analyses by us and others would seem to suggest that X-band observations would not prove to be very useful for such applications because of problems related to loss of coherence. In particular, the shorter wavelength (3.1 cm) pulse has been assumed to interact mostly with the upper vegetation canopy via volume scattering [11], [12]. This part of the canopy is easily affected by wind, hence, is not expected to maintain coherence even for short periods of time.

In this paper, we explore the feasibility of X-band TerraSAR-X (TSX) data for the wetland InSAR application. Surprisingly,

0196-2892/$26.00 © 2009 IEEE

Authorized licensed use limited to: Sang-Hoon Hong. Downloaded on January 27, 2010 at 07:15 from IEEE Xplore. Restrictions apply.

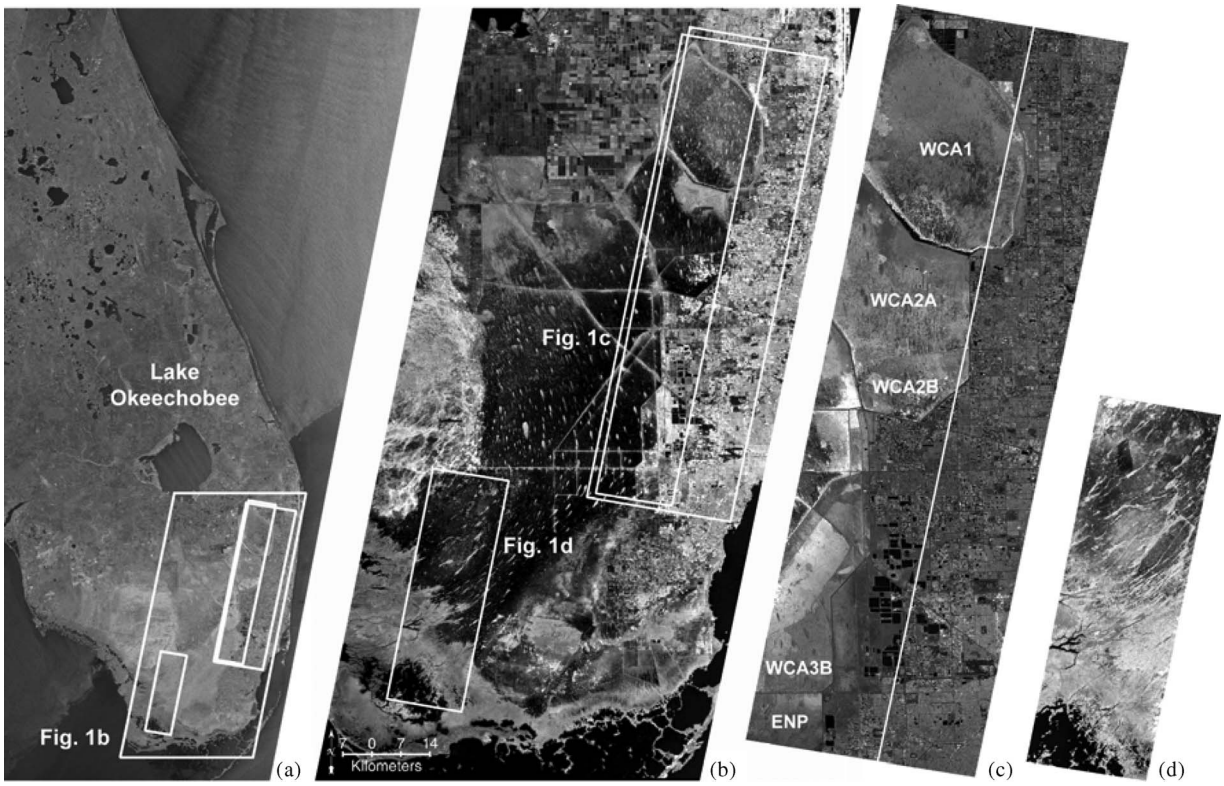

Fig. 1. SAR amplitude images showing the study area in eastern South Florida. (a) RADARSAT-1 ScanSAR image of Florida showing location of study area (RADARSAT data Canadian Space Agency / Agence Spatiale Canadienne 2002. Processed by CSTARS and distributed by RADARSAT International). (b) JERS-1 L-band amplitude image of eastern South Florida showing the location map of the TSX swathes. (c) TSX amplitude image of the northern study area consisting of both urban and wetland environments. The white line marks the eastern extent of the dual-polarization (HH + HV) swath, which is roughly half the width of the single-polarization (HH) swath. (d) TSX amplitude image of the southern study area consisting of saltwater (mangrove) and freshwater wetlands. Geographic locations: ENP—Everglades National Park; WCA1, WCA2A, WCA2B, and WCA3B—Water conservation areas 1, 2A, 2B and 3B.

our analysis demonstrates that X-band InSAR works quite well in wetlands and can be used for monitoring water-level changes in this challenging environment. Furthermore, we use dual-polarization data to evaluate the dominant scattering mechanism that enables the method to work with X-band data in wetlands, and find that volume scattering here may be less important than commonly believed.

II. Study Area

The Everglades in South Florida is a unique wetland environment consisting of a very wide, shallow, and slow sheetflow that drains Lake Okeechobee southward to the Gulf of Mexico [Fig. 1(a)]. Anthropogenic changes in the past 50 years have disrupted natural water flow and severely impacted the regional ecosystem. Currently, the northern section of the Everglades' flow is controlled by a series of structures (e.g., levees, gates) and serves mainly as water reservoir. In the southern section of the Everglades, the original wetland sheetflow has been preserved, although the water supply for the flow is controlled by the local water authorities. The surface water levels in the Everglades are monitored by probably the densest stage (water level) network in the world, consisting of more than 200 stations, spaced 5–10 km from one another. The Everglades' very wide flow combined with the dense stage network provides an almost perfect large-scale natural and controlled laboratory for testing space-geodetic hydrological technologies.

In this paper, we focused on two areas, a northern area located on the eastern edge of the managed wetlands [Fig. 1(c)] and a southern area located within the natural-flow wetlands [Fig. 1(d)]. The northern study area consists of two TSX consecutive frames. It was selected because it contains both wetland and urban environments, allowing us to compare the interferometric phase and coherence calculated for the two environments. The wetlands in this section of the Everglades are divided by a set of levees into five managed areas: Water Conservation Areas (WCA) 1, 2A, 2B, 3A, and 3B; these areas serve as water reservoirs for the large southeast Florida population (more than five million people). Due to the levees, gates, and other managed flow structures, water levels tend to vary significantly within a short distance and a short time, an excellent environment for testing new high-spatial-resolution monitoring techniques. The southwestern corner of the northern study area comprises of natural-flow wetlands, which are parts of the Everglades National Park (ENP). Based on our previous study [6], we do not expect a large signal over there because flow patterns in open areas are diffusive and harder to detect by InSAR.

The southern study area is located within the ENP across the transition between freshwater and saltwater (mangrove) wetlands. This area was selected to evaluate the suitability of the wetland InSAR application in different wetland environments, including woody (saltwater mangrove) and herbaceous (freshwater) vegetations. Furthermore, our previous L-band study showed detectable water-level changes (fringes) across

Authorized licensed use limited to: Sang-Hoon Hong. Downloaded on January 27, 2010 at 07:15 from IEEE Xplore. Restrictions apply.

TABLE I
LIST OF TSX DATA

Area	*Date*	*Polarization*	*Track*	*Incidence angle (degrees)*
WCA	2008-04-25	HH	T112_strip_006	28.8
WCA	2008-05-06	HH	T112_strip_006	28.8
WCA	2008-05-17	HH	T112_strip_006	28.8
WCA	2008-05-28	HH	T112_strip_006	28.8
WCA	2008-06-19	HH/HV	T112_stripFar_006	29.3
WCA	2008-06-30	HH/HV	T112_stripFar_006	29.3
WCA	2008-07-11	HH/HV	T112_stripFar_006	29.3
WCA	2008-07-22	VV/VH	T112_stripFar_006	29.3
WCA	2008-08-02	VV/VH	T112_stripFar_006	29.3
WCA	2008-08-13	VV/VH	T112_stripFar_006	29.3
WCA	2008-08-24	VV/VH	T112_stripFar_006	29.3
ENP	2008-09-15	HH/HV	T112_stripNear_008	32.7
ENP	2008-09-26	HH/HV	T112_stripNear_008	32.7
ENP	2008-10-07	HH/HV	T112_stripNear_008	32.7
ENP	2008-10-18	HH/VV	T112_stripNear_008	32.7
ENP	2008-10-29	HH/VV	T112_stripNear_008	32.7
ENP	2008-11-09	VV/VH	T112_stripNear_008	32.7
ENP	2008-11-20	VV/VH	T112_stripNear_008	32.7

WCA – Water Conservation Areas (managed wetlands);
ENP – Everglades National Park (natural-flow wetlands).

this transition induced by tide movement in the saltwater mangrove [6]. Thus, we expect to find here tide-induced water-level changes.

III. TSX DATA AND PROCESSING

Our analysis is based on three sets of TSX observations acquired over the two study areas during an eight-month period in 2008 (Table I). The first set consists of four consecutive acquisitions of the northern study area every 11-day repeat cycle between April 25, 2008 and May 28, 2008. The data was acquired in the standard stripmap mode with 3-m pixel resolution, 30-km-wide swath, and HH polarization. It is apparent that the high-resolution data show the sharp amplitude image [Fig. 1(c)] but also results in huge data files (about 2 GB per scene). The second set was acquired in a dual-polarization stripmap mode over the western half of the same area. It consists of three HH/HV and four VV/VH acquisitions with a 15-km-wide swath. Because interferograms can be usually generated with the same data type, we were able to generate three HH, three HV, six VV, and six VH interferograms. The third set was also acquired with dual-polarization stripmap mode over the southern study area. It consists of three HH/HV, two HH/VV, and two VV/VH acquisitions also with 15-km-wide swath. This set allowed us to generate ten HH, six VV, three HV, and one VH interferograms.

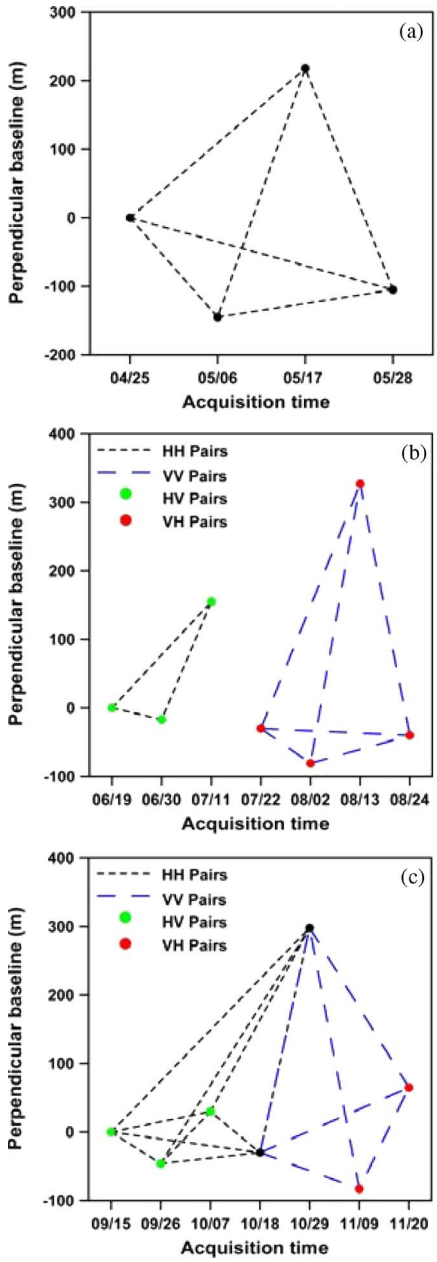

Fig. 2. Perpendicular baseline information with respect to the first acquisition of each TSX track. Dashed black and blue lines represent interferometric HH and VV pairs, respectively, used in this study. (a) Track T112_strip_006 with single HH polarization. (b) Track T112_stripFar_006 with the dual-polarization acquisitions. (c) Track T112_stripNear_008 showing dual-polarization acquisitions in the southern study area.

We processed the TSX data with the Repeat Orbit Interferometry PACkage software, which calculates repeat-pass interferograms using a digital elevation model (DEM) to eliminate topographic effects [13]. We calculated all possible interferograms, which include 19 HH, 12 VV, 6 HV, and 7 VH, a total of 44 interferograms. All interferograms show contained areas with sufficient interferometric coherence and were used in this study. Fringe patterns related to water level changes are detected in all interferograms, but the coherence levels are dependent on temporal decorrelation, polarization, and surface conditions. Our calculations include phase unwrapping [14], topographic phase removal based on the SRTM-1 DEM, and

Authorized licensed use limited to: Sang-Hoon Hong. Downloaded on January 27, 2010 at 07:15 from IEEE Xplore. Restrictions apply.

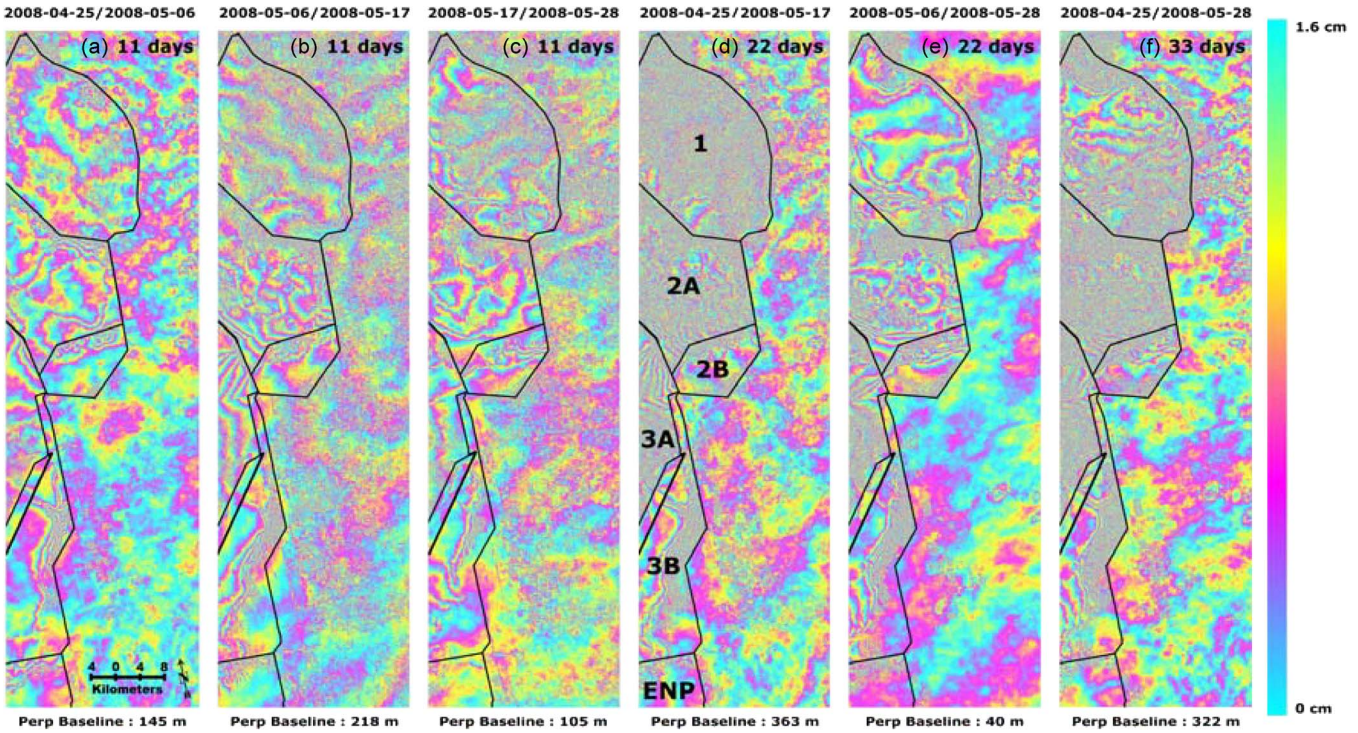

Fig. 3. TSX interferograms of wetlands and urban areas in southeast Florida. Each fringe cycle represents 1.6-cm change in the line of sight between the satellite and the surface, which translates into 2 cm of vertical movement. The short wavelength fringe patterns in the wetlands (western sections) reflect surface changes due to water-level changes. The longer wavelength fringe patterns in both urban and wetland environment reflects, most likely, atmospheric noise. All three 11-day interferograms [(a)–(c)] show that phase is maintained throughout the wetland area. The longer time span interferograms [(d)–(f)] show significant decorrelation over the wetlands. The lateral extent of the decorrelated area increased with the length of the perpendicular and temporal baselines.

filtering [15]. The temporal baselines of interferometric pairs are 11–55 days. The range of their geometric baselines perpendicular to a radar-look direction is from 40 to 420 m (Fig. 2). The small perpendicular baselines indicate that TSX orbits are well controlled and, hence, suitable for the wetland interferometric application.

IV. Results

A. Proof-of-Concept Study

This study is based on the first data set consisting of four HH stripmap acquisitions of the northern study area. The purpose of this study was testing the suitability of TSX for wetland InSAR applications. We used the four acquisitions to generate all six possible interferograms with time span of 11, 22, and 33 days (Fig. 3). All three 11-day interferograms [Fig. 3(a)–(c)] show that phase is maintained throughout the wetland area. The longer time span interferograms [Fig. 3(d)–(f)] show significant decorrelation over the wetlands. The lateral extent of the decorrelated area increases with the length of the perpendicular and temporal baselines.

The interferograms show two fringe patterns and differ from one another by their wavelength, shape, organization, and location. The first type is of short wavelength fringe pattern, well organized, and found only in the wetlands (western sections). These fringes reflect surface changes due to water-level changes. The longer wavelength fringes have a more diffusive pattern and are found in both urban and wetland environments. These fringes reflect, most likely, atmospheric noise.

The shape and patterns of the shorter wavelength fringes vary from one interferogram to the other and also between the different conservation areas, as water levels change daily and spatially due to rain events, evapotranspiration, and mainly due to managed flow. Some of the most interesting fringe patterns are very dense and organized fringe pattern in the northern part of area 3B [Fig. 4(a)], bull's-eye fringe pattern in WCA-2B [Fig. 4(b)], and high-gradient fringes in the western side of WCA-1 [Fig. 4(c)]. The high fringe gradient in area 3B reflects surface-water flow from the Miami Canal spillway into an open area conducted for wellfield recharge. The bull's-eye pattern in area 2B is very similar to a pattern we detected with L-band data [4], [6]. The pattern reflects dynamic water topography due to the southward flow in culverts connecting area 2A and 2B. Finally, the high fringe gradient in area WCA-1 represents surface flow from the western peripheral canal eastward into the heart of the conservation area.

The most robust method for evaluating the quality of InSAR observations is calculating coherence maps for the study area and comparing the coherence values of the various interferograms [16]. We conducted such coherence analysis with estimation window of 5 by 5 pixels (5 by 10 m) for all six interferograms and calculated the average coherence in wetlands and in urban areas (Fig. 5). Our analysis shows not only high coherence values in the urban area (> 0.44) but also relatively high coherence in wetlands (> 0.35). The coherence in wetlands shows strong dependence on the temporal baseline [Fig. 5(a)] and less dependence on the perpendicular one [Fig. 5(b)]. The inverse relations between wetland interferometric coherence

Authorized licensed use limited to: Sang-Hoon Hong. Downloaded on January 27, 2010 at 07:15 from IEEE Xplore. Restrictions apply.

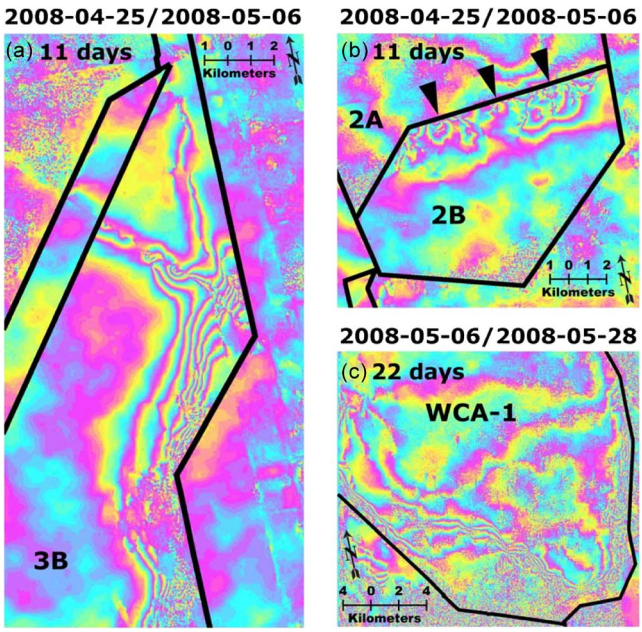

Fig. 4. Flow-induced elongated fringe patterns in the Everglades wetlands. (a) High-density fringes along the Miami Canal spillway and in an open area used for wellfield recharge. The water-level change is in the range of 0–15 cm (up to seven cycles). (b) Circular fringe patterns in the northern extent of WCA-2B induced by southward flow from WCA-2A through (marked by black triangles) three culverts located along the separating levee. (c) Northwest–southeast fringes in the southern section of WCA-1 reflecting water-level changes due to rapid flow in the peripheral canals and slow flow in the interior of the area where vegetation resistance govern the flow. Some areas in the southern section of WCA-1 are incoherent after 22 days because of the sparse herbaceous vegetation, which cannot maintain phase over long time span.

and temporal baseline are consistent with our previous study based on C- and L-band data [5], [8].

B. Multipolarization Study

After confirming that TSX HH polarization data is suitable for InSAR wetland applications, we expanded our study to explore the suitability of other polarization-data types to this application. To conduct this study, we acquired dual-polarization data over the two study areas experimenting with different polarization pairs: HH/HV, VV/VH, and HH/VV (Table I). Our main goal was using the phase data to calculate different polarization interferograms. However, we also used the amplitude data to investigate the relations between polarization data, vegetation type, and scattering mechanisms in wetlands.

Our multipolarization study of the northern study area shows short wavelength fringes in all four polarization interferogram (Fig. 6). The fringes are confined to hydrologic surface structures reflecting water-level changes in the managed wetlands. The high fringe gradient, particularly in WCA-2A, reflects high water levels in the wet season and rapid changes in surface water level due to managed flow between the conservation areas. The interferograms show that phase is maintained in almost all wetland areas. However, some small decorrelated areas appear in the cross-polarization interferograms. The intensity of the fringes, which is proportional to the coherence level, is much higher in the copolarization interferograms. Despite the intensity variations, the fringe patterns in the co- and cross-

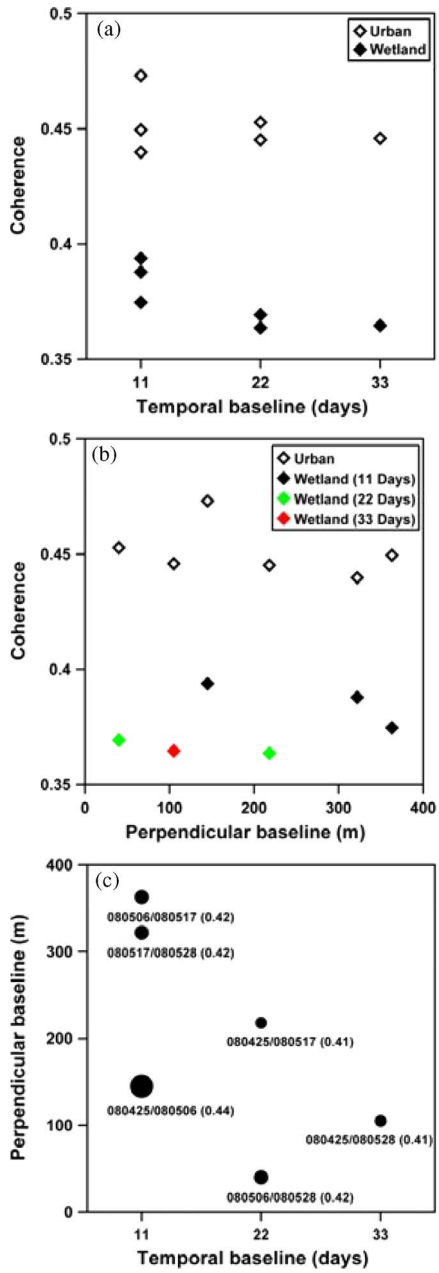

Fig. 5. Coherence analysis of the TSX interferometric data. The analysis shows not only high coherence values in the urban area (> 0.44) but also relatively high coherence in wetlands (> 0.35). The coherence in wetlands shows (a) strong dependence on the temporal baseline and (b) less dependence on perpendicular one.

polarization interferograms are very similar, suggesting that all polarization data reflect water-level changes in the wetlands. The fringe intensity level also varies spatially within each interferogram suggesting coherence dependence on vegetation type and density.

We also used the multipolarization amplitude information to map and evaluate the dominant scattering mechanism in different sections of the wetlands using decomposition methods. The scattering matrix in such methods is decomposed into components with meaningful physical properties to identify dominant scattering types. The widely used Pauli decomposition is a simple method that displays color composite images of the main three scattering types: odd scattering (blue, $S_{hh} + S_{vv}$),

Authorized licensed use limited to: Sang-Hoon Hong. Downloaded on January 27, 2010 at 07:15 from IEEE Xplore. Restrictions apply.

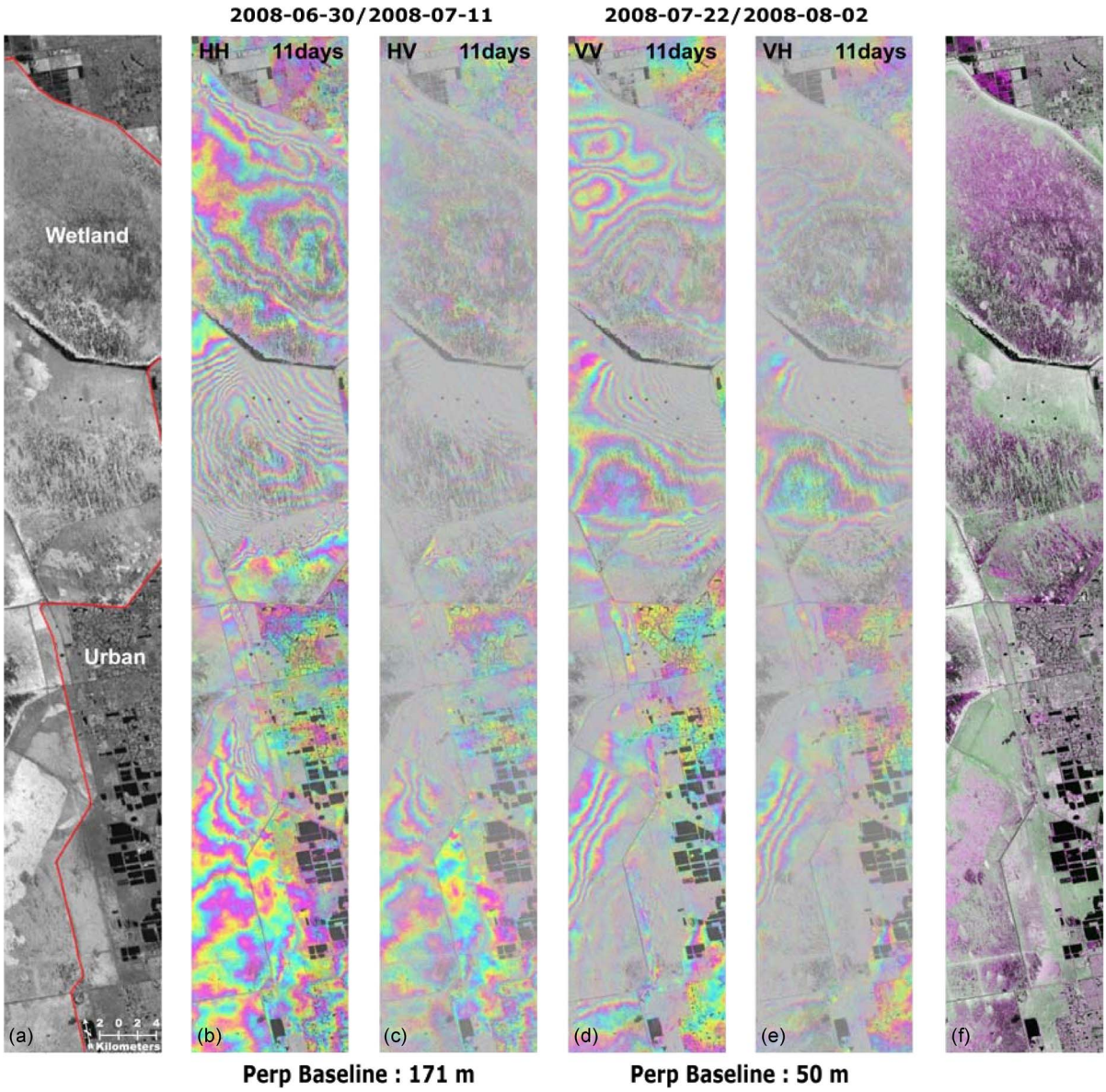

Fig. 6. SAR data and interferograms of the northern study area. (a) SAR amplitude image of the study area. The red line shows the boundary between the wetlands and the urban areas. (b)–(e) HH, HV, VV, and VH polarization interferograms, respectively. (f) Pauli decomposition of the amplitude data: red—HH–VV (even scattering—dihedral); green—HV (rotated dihedral); and blue—HH + VV (odd scattering).

even scattering (red, $S_{hh} - S_{vv}$), and rotated dihedral scattering (green, $2S_{hv}$) [17]–[20]. A proper Pauli decomposition requires a full quad-polarization data, which is still not available by TSX. Hence, we conducted a pseudoanalysis using two dual-polarization data. Our results show that the scattering in most of the wetland area is either even (red) or rotated dihedral (green), with very limited odd-scattering (blue) areas [Fig. 6(f)]. The even-scattering areas (red) are characterized by woody wetlands, whereas the rotated-dihedral (green) areas are characterized by herbaceous vegetation, mainly of sawgrass and cattail. Interestingly, the fringe color intensity (coherence) is higher in red (even scattering) areas than in the green areas (rotated dihedral). Furthermore, coherence loss occurs mainly in areas mapped by dark green, where the radar signal is dominated by rotated dihedral (HV).

We conducted a similar interferometric and amplitude analyses for the multipolarization data acquired over the southern study area (Fig. 7). The HH and HV interferograms of September 26, 2008/October 7, 2008 pair show a high fringe gradient in the saltwater (mangrove) area, which may reflect water-level change induced by ocean tides [6]. In the HH and VV interferograms of October 18, 2008/November 9, 2008 pair, the HH interferogram shows a clearer fringe pattern related to water-level changes compared with VV interferogram. The VV and VH interferograms of November 9, 2008/November 20, 2008 pair do not show such signal, most likely because both acquisitions were obtained in similar tide conditions. The copolarization interferograms show high coherence (color intensity) in both saltwater and freshwater wetlands. However, the cross-polarization interferograms indicate very low coherence in freshwater areas, which are characterized by herbaceous vegetation, but sufficient coherence in the saltwater mangrove areas. We also conducted the Pauli decomposition showing that the freshwater herbaceous area is dominated by even scattering

Authorized licensed use limited to: Sang-Hoon Hong. Downloaded on January 27, 2010 at 07:15 from IEEE Xplore. Restrictions apply.

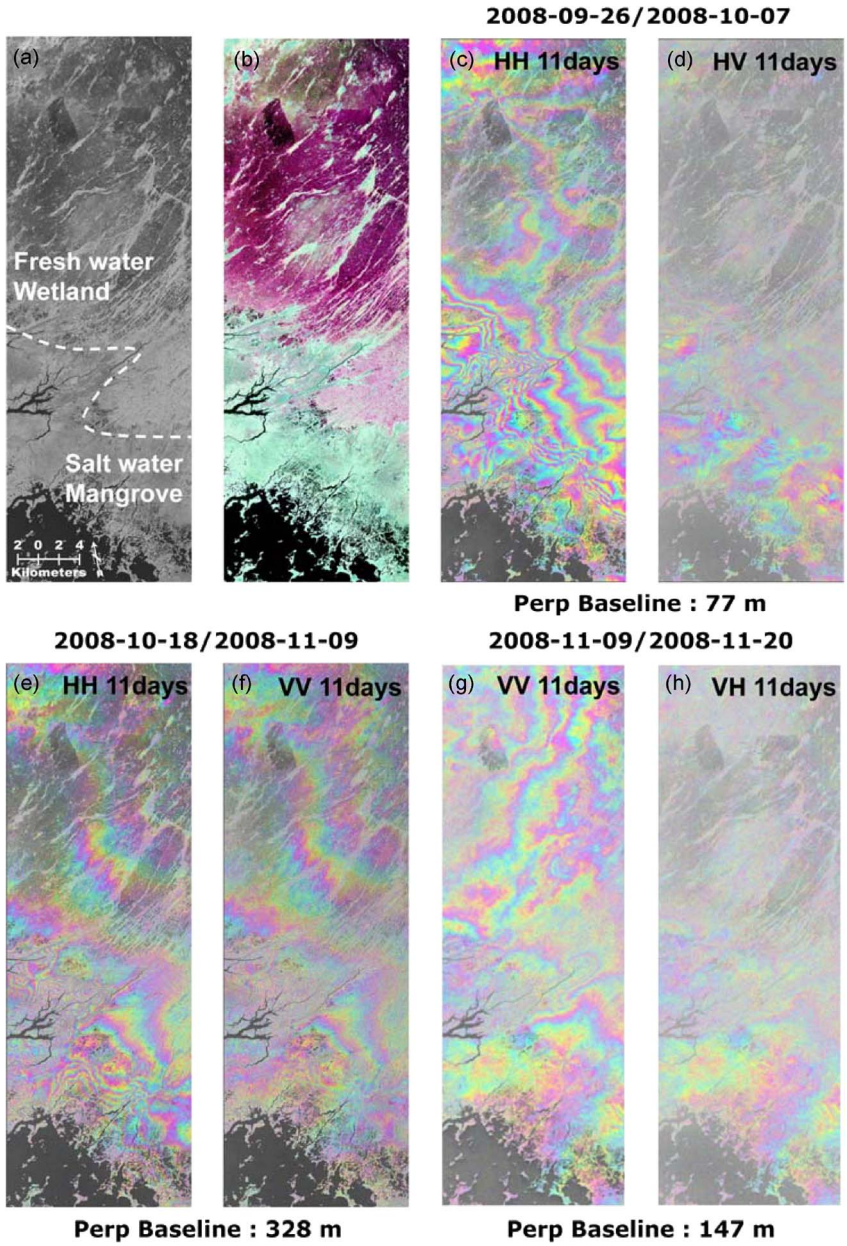

Fig. 7. SAR data and interferograms of the southern study area. (a) SAR amplitude image of the study area. The dashed line shows the boundary between the fresh- and salt-water wetlands. (b) Pauli decomposition of the amplitude data: red—HH–VV; green—HV; and blue—HH + VV. (c)–(h) HH, HV, VV, and VH polarization interferograms.

(red), and the saltwater mangrove area is dominated by rotated dihedral scattering (green).

The four polarization interferograms in both study areas show different level of coherence as shown by the color intensity of the interferogram (Figs. 6 and 7). To compare the coherence of the different polarization interferograms, we calculated average coherence values for the entire study areas, as well as separate values for the wetland and urban sections of the northern study area [Fig. 6(a)]. Overall, coherence values in both areas and for all polarization interferograms are high (> 0.42; Fig. 8). Highest values are obtained in the copolarization interferograms, in which the HH coherence is higher than the VV coherence. The cross-polarization interferograms show lowest coherence values. The multipolarization coherence analysis confirms our previous proof-of-concept results. We found that the coherence in urban areas is significantly higher than in wetlands in all four polarizations [Fig. 8(a)]. In addition, we detected the same inverse relation between coherence and temporal baseline in all four polarization interferograms [Fig. 8(b)]. A comparison between Figs. 5 and 8 in both wetland and urban areas shows that the coherence levels of dual-polarization stripmap mode are higher than those of the standard stripmap mode data by $\sim$10%. Because we conducted exactly the same coherence analysis in both cases, we suspect that the observed coherence differences are related to the pixel resolution used in each acquisition mode. Azimuth pixel resolution in standard stripmap mode is 3 m whereas in dual-polarization mode is 6 m.

Authorized licensed use limited to: Sang-Hoon Hong. Downloaded on January 27, 2010 at 07:15 from IEEE Xplore. Restrictions apply.

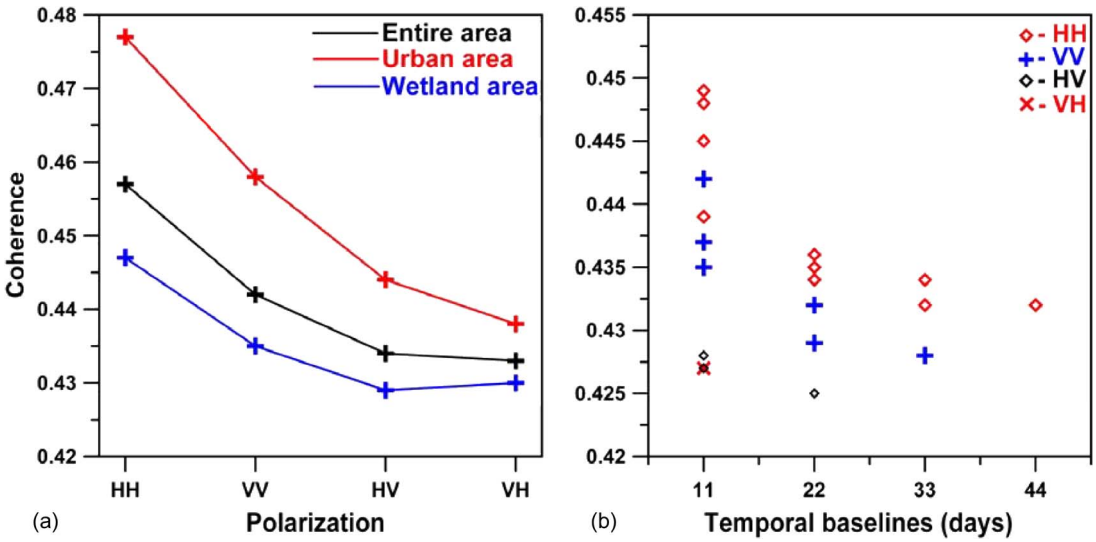

Fig. 8. Coherence analysis of the TSX co- and cross-polarization interferometric data, showing overall high coherence values in all four polarization interferograms (> 0.4). (a) Average coherence in northern study area comprising of managed wetlands and urban area. (b) Average coherence in southern study area covered with freshwater herbaceous and saltwater mangrove wetlands. The analysis shows higher coherence in the urban area than in wetlands and an overall reduction in coherence from co- to cross-polarization. Because HV and VH acquisitions were obtained in different times, the HV and VH are not identical and as suggested by theory. Interestingly, HV values are higher than VH values in urban areas but lower in wetlands.

V. Discussion and Conclusion

The most important outcome of this study is the surprising result that wetland InSAR has work well with X-band TSX data. Heretofore, it was assumed that the shorter X-band wavelength (3.1 cm) radar pulse interacts mostly with upper sections of the vegetation, such as canopies and branches, which are moved frequently by wind and, hence, are not good stable scatterers over time for InSAR. However, our results have clearly shown that X-band interferograms are coherent over wetland, suggesting stable scattering sources over time periods of at least 11 days. Hence, our results have ruled out volume scattering from canopies and branches as the dominant scattering mechanism in wetland environments.

Previous studies suggested that wetland InSAR works due to the "double-bounce" effect [21], in which the radar pulse is backscattered twice from the water surface and vegetation [1], [4]. The four polarization interferograms in the multipolarization study have also shown high coherence with highest values in HH, then VV, and lowest in HV or VH. All polarization interferograms have shown very similar fringe patterns, suggesting that that all polarization data reflect water-level changes in wetlands. Sensitivity of the radar pulse to water-level change can occur only if the pulse scatters from the water surface. Thus, we suggest that the dominant scattering mechanism in wetland environment is multiple bounce, double or more, in which one of the bounces occurs from the water surfaces. Multiple bounces also dominate the rotated dihedral cross-polarization signal (HV or VH), which is also indicative of water-level changes.

The different interferograms have shown strong relations between fringe patterns and hydrological structures (Figs. 3, 4, and 6), suggesting that the observed phase changes are induced by surface water-level changes. Due to a dense network of stage (water level) stations in the Everglades, we can verify that the InSAR-detected surface changes indeed correspond to water-level changes. We present here one example of a validation/calibration study using the HH interferogram calculated for the dates June 30, 2008/July 11, 2008 [Fig. 6(b)]. The first step in this analysis is conversion of the unwrapped phase information into water-level changes. Based on the incidence angle (29.3°) and wavelength (3.1 cm), we calculated a 1.8-cm vertical movement for each phase cycle $(1.8\ \text{cm} = \text{half-wavelength}/[\cos(\text{incidence angle})])$, assuming that all the displacement is vertical. The InSAR-based map of water-level changes shows variable change values with maximum changes of 30 cm in WCA-2A [Fig. 9(a)]. The actual validation/calibration procedure is conducted for each WCA separately [Fig. 9(b)–(d)] because water levels are discontinuous across the levees separating one area from the other. Stage data used in this procedure [Fig. 9(c)] also show maximum changes of 30 cm in WCA-2A similar to the InSAR-based water-level changes. We use a best fit analysis with a slope of one $(y = a + x)$ to calculate the offset between the two data sets. Some stage stations located in canals are not used for the calibration procedure because of low coherences in InSAR map and due to near-field flow dynamics that bias the stage data [22]. The same best fit analysis allows us to calculate the root-mean-square errors for each area which is in the range of 2–4 cm. A detailed description of this procedure is provided by [6]. The calibration/validation procedure here shows an overall very good fit between the InSAR-detected and the stage data indicating that TSX can be used to detect and monitor surface water-level changes in wetland with accuracy of 2–4 cm.

The usefulness of the X-band data for the wetland application, detection of water-level changes, still requires further evaluation. The advantages of the TSX data are the following: very high pixel resolution (1–3 m), short repeat orbit interval (11 days), data acquisition with different polarization parameters, and high detection level reflecting the 3.1 cm wavelength of the TSX radar system. These properties can be very useful

Authorized licensed use limited to: Sang-Hoon Hong. Downloaded on January 27, 2010 at 07:15 from IEEE Xplore. Restrictions apply.

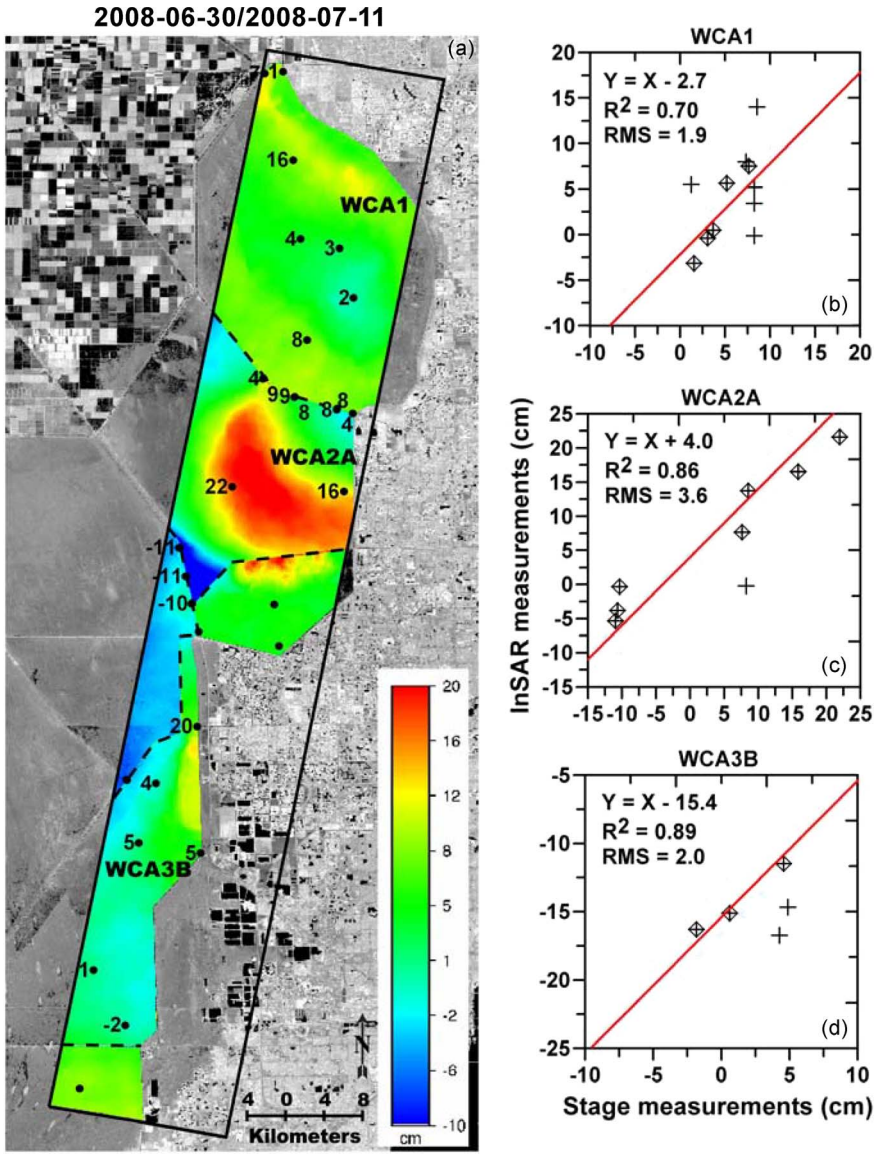

Fig. 9. Validation and calibration of the InSAR-detected water-level changes using stage (water level) information. (a) Map showing the InSAR-detected water-level changes, (black dots) stage-station locations, and [(b)–(d)] stage detected values at the stations. Calibration plots of water-level changes in three conservation areas. The red line denotes a line with a slope of one $(y = a + x)$ that best fits the data and to calibrate the offset between the InSAR and the stage observations. The "+" marks stations located in canals that do not represent well-water levels in the vegetated wetland and, hence, are not used for the calibration analysis.

for monitoring detailed flow patterns, such as the effect of channels as conduits in wetlands. The disadvantages of the TSX data are the following: small coverage area (10–30-km-wide swath) and possible fringe saturation in areas with high gradient of water-level changes. These limitations of the TSX system suggest that TSX data should not be used in the same way as the wider swath C- and L-band systems, which cover large wetland areas. The very high resolution TSX data should be used wisely for localized targets that need detailed information, such as the relationships between wetland and channel flow.

ACKNOWLEDGMENT

The authors would like to thank T. Dixon for useful discussions and comments, the three anonymous reviewers for their helpful constructive reviews, the German Aerospace Center for access to the TSX data, and the South Florida Water Management District and the U.S. Geological Survey for access to stage data. This is Center for Southeastern Tropical Advanced Remote Sensing (CSTARS) contribution No. 25.

REFERENCES

[1] D. E. Alsdorf, J. M. Melack, T. Dunne, L. A. K. Mertes, L. L. Hess, and L. C. Smith, "Interferometric radar measurements of water level changes on the Amazon flood plain," *Nature*, vol. 404, no. 6774, pp. 174–177, Mar. 9, 2000.

[2] D. E. Alsdorf, L. C. Smith, and J. M. Melack, "Amazon floodplain water level changes measured with interferometric SIR-C radar," *IEEE Trans. Geosci. Remote Sens.*, vol. 39, no. 2, pp. 423–431, Feb. 2001.

[3] D. Alsdorf, C. Birkett, T. Dunne, J. Melack, and L. Hess, "Water level changes in a large Amazon lake measured with spaceborne radar interferometry and altimetry," *Geophys. Res. Lett.*, vol. 28, no. 14, pp. 2671–2674, Jul. 15, 2001.

[4] S. Wdowinski, F. Amelung, F. Miralles-Wilhelm, T. H. Dixon, and R. Carande, "Space-based measurements of sheet-flow characteristics in the Everglades wetland, Florida," *Geophys. Res. Lett.*, vol. 31, no. 15, p. L15503, Aug. 7, 2004.

Authorized licensed use limited to: Sang-Hoon Hong. Downloaded on January 27, 2010 at 07:15 from IEEE Xplore. Restrictions apply.

[5] S. Wdowinski, S.-W. Kim, F. Amelung, and T. Dixon, "Wetland InSAR: A new space-based hydrological monitoring tool of wetlands surface water level changes," in *Proc. GlobWetland Symp.*, 2006.
[6] S. Wdowinski, S. W. Kim, F. Amelung, T. H. Dixon, F. Miralles-Wilhelm, and R. Sonenshein, "Space-based detection of wetlands' surface water level changes from L-band SAR interferometry," *Remote Sens. Environ.*, vol. 112, no. 3, pp. 681–696, Mar. 18, 2008.
[7] S.-W. Kim, S. Wdowinski, F. Amelung, and T. H. Dixon, "C-band interferometric SAR measurements of water level change in the wetlands: Examples from Florida and Louisiana," in *Proc. IGARSS*, Seoul, Korea, 2005, pp. 2708–2710.
[8] Z. Lu and O. I. Kwoun, "Radarsat-1 and ERS InSAR analysis over southeastern coastal Louisiana: Implications for mapping water-level changes beneath swamp forests," *IEEE Trans. Geosci. Remote Sens.*, vol. 46, no. 8, pp. 2167–2184, Aug. 2008.
[9] S. W. Kim, S. H. Hong, and J. S. Won, "An application of L-band synthetic aperture radar to tide height measurement," *IEEE Trans. Geosci. Remote Sens.*, vol. 43, no. 7, pp. 1472–1478, Jul. 2005.
[10] S. K. Lee, S. H. Hong, S. W. Kim, Y. Yamaguchi, and J.-S. Won, "Polarimetric features of oyster farm observed by AIRSAR and JERS-1," *IEEE Trans. Geosci. Remote Sens.*, vol. 44, no. 10, pp. 2728–2735, Oct. 2006.
[11] H. Hirosawa, Y. Matsuzaka, and O. Kobayashi, "Measurement of microwave backscatter from a cypress with and without leaves," *IEEE Trans. Geosci. Remote Sens.*, vol. 27, no. 6, pp. 698–701, Nov. 1989.
[12] E. Mougin, A. Lopes, M. A. Karam, and A. K. Fung, "Effect of tree structure on X-band microwave signature of conifers," *IEEE Trans. Geosci. Remote Sens.*, vol. 31, no. 3, pp. 655–667, May 1993.
[13] S. M. Buckley, P. A. Rossen, and P. Persaud, *ROI_PAC Documentation—Repeat Orbit Interferometry Package*, 2000.
[14] C. W. Chen and H. A. Zebker, "Two-dimensional phase unwrapping with use of statistical models for cost functions in nonlinear optimization," *J. Opt. Soc. Amer. A, Opt. Image Sci. Vis.*, vol. 18, no. 2, pp. 338–351, Feb. 2001.
[15] R. M. Goldstein and C. L. Werner, "Radar interferogram filtering for geophysical applications," *Geophys. Res. Lett.*, vol. 25, no. 21, pp. 4035–4038, Nov. 1, 1998.
[16] A. Monti Guarnieri and C. Prati, "SAR interferometry: A 'quick and dirty' coherence estimator for data browsing," *IEEE Trans. Geosci. Remote Sens.*, vol. 35, no. 3, pp. 660–669, May 1997.
[17] V. Karathanassi and M. Dabboor, "Land cover classification using ESAR polarimetric data," in *Proc. XXth ISPRS Congr. Comm. VII*, Istanbul, Turkey, 2004, pp. 280–285.
[18] S. R. Cloude and E. Pottier, "A review of target decomposition theorems in radar polarimetry," *IEEE Trans. Geosci. Remote Sens.*, vol. 34, no. 2, pp. 498–518, Mar. 1996.
[19] W. M. Boerner, H. Mott, E. Lunenburg, C. Livingstone, B. Brisco, R. J. Brown, and J. S. Patterson, *Principles and Applications of Imaging Radar, Manual of Remote Sensing*. New York: Wiley, 1998, ch. 5.
[20] M. Hellmann, "Classification of full polarimetric SAR data for cartographic application," Ph.D. dissertation, Tech. Univ. Dresden, Dresden, Germany, 1999.
[21] J. A. Richards, P. W. Woodgate, and A. K. Skidmore, "An explanation of enhanced radar backscattering from flooded forests," *Int. J. Remote Sens.*, vol. 8, no. 7, pp. 1093–1100, Jul. 1987.
[22] S. Lin and R. Gregg, "Water budget analysis water conservation area 1," South Florida Water Manage. District, West Palm Beach, FL, DRE 245, Jun. 1988.

Sang-Hoon Hong (S'03–M'07) received the B.S. and M.S. degrees in geological sciences and the Ph.D. degree in earth system sciences from Yonsei University, Seoul, Korea, in 1997, 1999, and 2006, respectively.

He is currently working as a Postdoctoral Associate Researcher with the Division of Marine Geology and Geophysics, University of Miami, Miami, FL, and also with the College of Engineering and Computing, Florida International University, Miami. His research interests include radar interferometry, radar polarimetry, and microwave signal processing. He has applied these synthetic aperture radar (SAR) and interferometric SAR techniques for the study of geodetic-change observation.

Shimon Wdowinski received the B.Sc. degree in earth sciences and the M.Sc. degree in geology from the Hebrew University, Jerusalem, Israel, in 1983 and 1985, respectively, and the M.S. degree in engineering sciences and the Ph.D. degree in geophysics from Harvard University, Boston, MA, in 1988 and 1990, respectively.

He is currently a Research Associate Professor with the Division of Marine Geology and Geophysics, Rosenstiel School of Marine and Atmospheric Science, University of Miami, Miami, FL. He is a Principal Investigator of projects funded by the National Aeronautics and Space Administration, the European Space Agency, Canadian Space Agency, German Space Agency, and Italian Space Agency on studies using synthetic aperture radar (SAR) and interferometric SAR observations for wetland research. His research has focused on the development and usage of space-geodetic techniques that can detect very precisely small movements of the Earth's surface. He has successfully applied these technologies to study natural hazards and environmental phenomena, such as earthquakes, sea-level rise, landslides, urban subsidence, and wetland surface flow.

Sang-Wan Kim (S'00–M'05) received the Ph.D. degree in earth system sciences from Yonsei University, Seoul, Korea, in 2004. His Ph.D. thesis was on the analysis of subsidence in the urban area using permanent scatterer and volcano monitoring using differential synthetic aperture radar (SAR) interferometry.

He was a Postdoctoral Researcher with the Center for Southeastern Tropical Advanced Remote Sensing, University of Miami, Miami, FL. He is currently with the Department of Geoinformation Engineering, Sejong University, Seoul, Korea. His main research interests are in SAR data processing and the application of SAR interferometry.

Authorized licensed use limited to: Sang-Hoon Hong. Downloaded on January 27, 2010 at 07:15 from IEEE Xplore. Restrictions apply.